Volcano-Magnetic Signal Reveals Rapid Evolution of the Inner Structure of Piton de la Fournaise

Lydie Gailler, Philippe Labazuy, Quentin Dumont, Jean-luc Froger, Aline Peltier, Anthony Finizola, Valérie Cayol, Marie Chaput, Edouard Régis

JGR Solid Earth

RESEARCH ARTICLE
10.1029/2022JB025290

Special Section:
Advances in understanding volcanic processes

Volcano-Magnetic Signal Reveals Rapid Evolution of the Inner Structure of Piton de la Fournaise

Lydie Gailler[1], Philippe Labazuy[1], Quentin Dumont[1], Jean-Luc Froger[2], Aline Peltier[3,4], Anthony Finizola[3,5], Valérie Cayol[1], Marie Chaput[6,7], Edouard Régis[8], and The SlideVolc ERT Team[9]

[1]Université Clermont Auvergne, CNRS, IRD, OPGC, Laboratoire Magmas et Volcans, Clermont-Ferrand, France, [2]Université Jean Monnet - Faculté des Sciences et Techniques, Laboratoire de géologie de Lyon: Terre, Planètes, Environnement - UMR CNRS 5276 LGL-TPE, Lyon, France, [3]Université Paris Cité, Institut de Physique du Globe de Paris, CNRS, Paris, France, [4]Observatoire Volcanologique du Piton de la Fournaise, Institut de Physique du Globe de Paris, La Plaine des Cafres, France, [5]Laboratoire Géosciences Réunion, Université de La Réunion, Saint-Denis, France, [6]Stratagem974, Sainte Clotilde, France, [7]Now at BRGM Réunion, Saint-Denis, France, [8]Université Clermont Auvergne, CNRS, Observatoire de Physique du Globe de Clermont, Clermont-Ferrand, France, [9]See Appendix A

Abstract Near-real time analysis of magnetization can provide important information for the imaging of volcano systems and their spatiotemporal evolution. This study focuses on the contribution of volcano-magnetic signals from reiterations of ground magnetic measurements to investigate the evolution of active structures at the Piton de la Fournaise volcano from 2017 to 2020. Changes are demonstrated by magnetic anomalies along a reference profile by means of the reiteration periods. These variations are first modeled qualitatively in 2D using electrical resistivity constraints in order to investigate the evolution of magnetization at depth through time, and the model is subsequently compared with the 3D intrusive activity from depth up to the surface from Interferometric Synthetic Aperture Radar (InSAR) inverse modeling. The shallow areas of demagnetization modeled from one reiteration to another are consistent with the geometry and location of the underlying intrusions revealed by the 3D InSAR models, suggesting strong thermal, stress, and electrokinetic effects due to magmatic activity not only at the surface but also at depth, along the main magmatic paths. It also raises a question as to the extent of the associated thermal diffusion processes at the scale of individual magma injections. This study confirms that detecting resistivity and magnetization anomalies, and quantifying their spatiotemporal evolution, can provide powerful tools for imaging volcanic systems at various scales and for providing warning of associated hazards. It also highlights the necessity for 4D monitoring of volcanic edifices using this method to provide greater precision, an important issue that is now made possible by the use of Unmanned Aerial Vehicle measurements.

Plain Language Summary Volcanic activity (through volcano-tectonic, magmatic, and hydrothermal processes) undeniably disturbs the magnetic field, especially at a local scale. Recent studies have evidenced the potential of magnetic field measurements in imaging thermal anomalies (strong influence of temperature on magnetic measurements) and mechanical heterogeneities (fracturing-alteration). Piton de la Fournaise (La Réunion Island, Indian Ocean) is an outstanding target to address such issues, being highly active and closely monitored. In this study, we used repeated magnetic measurements conducted over 3 years along a 3,780-m-length profile close to the summit of Piton de la Fournaise. We used the complementarities between magnetization and electrical resistivity parameters in a 2D magnetic modeling approach, in order to image the consequence of the eruptive dynamics on the edifice structure at depth. The temporal evolution of the magnetic anomalies appears strongly correlated to the depths and volumes of magmatic intrusions along the main active area. These results open new perspectives in studying the spatiotemporal changes in magmatic, hydrothermal, and mechanical changes and alteration processes within volcanic edifices.

Key Points:

- Volcano-magnetic variations at Piton de la Fournaise volcano (magmatic and mechanical changes, hydrothermal alteration processes)
- 2D modeling of magnetic anomalies evolution under electrical resistivity constraints consistent with Interferometric Synthetic Aperture Radar 3D intrusions models
- Imaging the main paths of weakness at depth that could be associated with potential future magmatic transfers

Correspondence to:
L. Gailler,
l.gailler@opgc.univ-bpclermont.fr

Citation:
Gailler, L., Labazuy, P., Dumont, Q., Froger, J.-L., Peltier, A., Finizola, A., et al. (2023). Volcano-magnetic signal reveals rapid evolution of the inner structure of Piton de la Fournaise. *Journal of Geophysical Research: Solid Earth*, *128*, e2022JB025290. https://doi.org/10.1029/2022JB025290

Received 29 JUL 2022
Accepted 25 DEC 2022

Author Contributions:
Conceptualization: Lydie Gailler, Aline Peltier, Anthony Finizola, Marie Chaput, Edouard Régis
Formal analysis: Lydie Gailler, Philippe Labazuy, Quentin Dumont
Funding acquisition: Lydie Gailler, Philippe Labazuy, Aline Peltier
Investigation: Lydie Gailler, Philippe Labazuy, Quentin Dumont, Aline Peltier, Anthony Finizola, Marie Chaput, Edouard Régis

1. Introduction

Volcanic edifices are created by the complex superimposition and juxtaposition of diverse volcanic materials which can have contrasting mechanical properties (e.g., hardness, porosity, and degree of alteration). These materials are generally crosscut by structural discontinuities or weakness zones (such as faults or altered areas). The resulting complex 3D structure is subject to both regional and local stresses, induced for example, by

Methodology: Lydie Gailler, Philippe Labazuy, Quentin Dumont, Valérie Cayol, Marie Chaput
Project Administration: Aline Peltier, Anthony Finizola
Resources: Lydie Gailler, Philippe Labazuy, Aline Peltier, Anthony Finizola
Software: Jean-Luc Froger
Supervision: Lydie Gailler, Aline Peltier, Anthony Finizola
Validation: Lydie Gailler, Philippe Labazuy, Quentin Dumont, Jean-Luc Froger, Aline Peltier, Anthony Finizola
Visualization: Lydie Gailler, Philippe Labazuy, Jean-Luc Froger, Aline Peltier, Anthony Finizola, Valérie Cayol
Writing – original draft: Lydie Gailler
Writing – review & editing: Lydie Gailler, Philippe Labazuy, Quentin Dumont, Jean-Luc Froger, Aline Peltier, Anthony Finizola, Valérie Cayol

magmatic or hydrothermal fluid transfer. All these components interact at different scales, both in time and space, and play an important role both in the expression of volcanic activity and in the long-term evolution of volcanic edifices.

Therefore, imaging the 3D structure of volcano edifices and their evolution through time is both a real challenge and a crucial key to improving current constraints on the geometry and dynamics of the various processes affecting the eruptive precursors of active volcanoes, their instability phenomena (e.g., Hawaii: Lipman et al., 1988; Moore et al., 1994; Swanson et al., 2012; Stromboli: Finizola et al., 2009; Etna: Nicolosi et al., 2014; Piton de la Fournaise: Chaput et al., 2019), and surface manifestations and associated impacts (e.g., lava flood zones, gravity-driven tsunamis, and volcanic plume hazards; Labazuy et al., 2012; Millington et al., 2012).

A number of geophysical methods are well suited to imaging the 3D structures within an edifice (with good spatial resolution). Due to being easily repeatable, they are also useful for imaging the temporal evolution and dynamics of these structures. Some of them could therefore be highly important methods for investigating magma processes and their impacts on the structure of an edifice at different depths. For example, numerous studies have shown that volcanic activity (through volcano-tectonic, magmatic, and hydrothermal processes) clearly disturbs the magnetic field, especially on a local scale (e.g., Adler et al., 1999; Zlotnicki & Le Mouel, 1988; Zlotnicki & Le Mouél, 1990; Zlotnicki et al., 1993). Volcano-magnetic signals are commonly observed during the onset of seismic crises or eruptions and could be efficiently recorded through time series or reiterations. Magnetization is very sensitive to mineral alterations and temperature fluctuations and has proven to be very effective in monitoring the thermal state of volcanic edifices at depth (Bouligand et al., 2019; Brothelande et al., 2016; L. Gailler & Kauahikaua, 2018). So a magma intrusion, which induces high temperature fluid circulation as well as stress variations within the edifice, will have a demagnetizing effect on its environment. Similarly, electrical resistivity tomography (ERT) is particularly well suited for imaging the shallow structure (i.e., the upper few hundred meters) of a volcanic edifice (e.g., L. Gailler et al., 2019; Revil et al., 2018) and provides information on the electrical properties of the ground, particularly its fluid content. On the other hand, deformation measurements provide information on the geometry and pressurization of magma reservoirs and magma sheets such as dykes and sills.

Piton de la Fournaise (La Réunion Island, Indian Ocean) is an outstanding site for exploring these issues, as it not only has several eruptions each year but is also closely monitored using multidisciplinary observations from the Observatoire Volcanologique du Piton de la Fournaise from Institut de Physique du Globe de Paris (OVPF/IPGP). Observational data such as GNSS, Interferometric Synthetic Aperture Radar (InSAR), and tiltmeter measurements provide crucial constraints for deformation structures (i.e., movement of fluids and volume of intruding magma) and stress perturbations within the volcano edifice. Continuous seismic measurements also provide fundamental constraints on the dynamic processes. In addition, various research programs are currently underway on Piton de la Fournaise to provide improved imaging of the edifice's inner structure and increased understanding of the evolution of mechanical heterogeneities caused by physical processes. Geophysical measurements such as gravity (L. Gailler et al., 2009; Malengreau et al., 1999), magnetism (L.-S. Gailler & Lénat, 2012; Galdéano et al., 1988), magnetotelluric (L.-S. Gailler et al., 2018), and deformation (e.g., Q. Dumont et al., 2022; Froger et al., 2015; Fukushima et al., 2010; Peltier et al., 2005, 2009; Smittarello et al., 2019) also provide strong constraints on the structure and dynamics of the volcano. In this paper, we focus on electrical resistivity and magnetism measurements carried out to image the consequences of the eruptive dynamics on the edifice structure at depth. This can be used to help provide constraints on the main paths of weakness at depth that could be associated with potential future magma transfer.

Here, we present data sets acquired during three magnetic measurement surveys that were carried out along a profile across the N-NE flank of the Piton de la Fournaise volcano between 2017 and 2020. We clearly identify temporal variations in the magnetic anomalies between each of the reiteration periods. We therefore performed 2D magnetic models using constraints from a large-scale ERT profile carried out in 2017, that is, at the beginning of the magnetic measurements. The geometry of 3D magmatic injections deduced from InSAR displacement data was also used to compare the evolution of modeled heterogeneities in shallow magnetization and the inferred magma paths during the periods concerned. The resulting models and the main axes of demagnetization reflect a rapid evolution of the inner structures, possibly driven by fluid transfer (i.e., magmatic and hydrothermal) within the edifice, at the time of eruption.

2. Geological and Geophysical Background

2.1. Eruptive Context of Piton de la Fournaise Volcano

Piton de la Fournaise volcano is one of the most active volcanoes in the world with a mean of two eruptions per year. As commonly documented for oceanic basalt volcanoes (MacDonald, 1972), magma transfer is first initiated vertically before propagating laterally along rift zones (RZs; e.g., Peltier et al., 2009) radiating from the summit at Dolomieu crater. These preferential intrusion paths have been determined at the surface from the locations and orientations of superficial markers such as scoria cones, cinder cones, and eruptive fissures (Bonali et al., 2011; Michon et al., 2016; Villeneuve & Bachèlery, 2006). A recent image of the intrusion geometry at depth, based on a compilation of inverse displacement modeling for 57 magma injections that occurred between 1998 and 2020 (Q. Dumont et al., 2022), provides better definition of the internal structure of the RZ on the scale of the overall edifice.

Various structures have been identified at Piton de la Fournaise: (a) two main RZs (northeast, NERZ; southeast, SERZ) and two less active intrusive directions (N120 RZ and N60 RZ) as described in Bachèlery (1981) and Michon et al. (2015); (b) a highly active hydrothermal system situated about 300 m below the Central Cone (e.g., Barde-Cabusson et al., 2012; M. Dumont et al., 2019; J.-F. Lénat & Bachèlery, 1990; J.-F. Lénat, Bachèlery, & Merle, 2012); (c) a shallow magma plumbing system located between about 0 and 500 m a.s.l. from which dykes/sills initiate (e.g., J. F. Lénat & Bachèlery, 1988; Michon et al., 2015; Peltier et al., 2009); and (d) an active sliding plane beneath the eastern flank (e.g., Q. Dumont et al., 2022) with evidence of partial collapses in the past (e.g., Labazuy, 1996; Oehler et al., 2004).

Eruptive activity at Piton de la Fournaise is always associated with individual shallow dyke injections and is marked by different geometries depending on the RZs in which they occur (e.g., Q. Dumont et al., 2022; Peltier et al., 2009). Ninety-five percent of the historical eruptive activity has occurred within the uninhabited Enclos Fouqué caldera (Figure 1, e.g., Chevrel et al., 2021). The risk of eruptions in inhabited areas outside the caldera, while not high (12 times since the eighteenth century; Chevrel et al., 2021), should also be taken into account. Phreatomagmatic eruptions have also been reported occasionally inside the Dolomieu crater, with 17 events since the eighteenth century (Villeneuve & Bachèlery, 2006).

In this study we focus on the eruptive activity of the May 2017 to November 2020 period, that is, the period covered by our magnetic measurements. During this period, a total of 18 shallow magma injections (13 eruptions and 5 intrusions that did not reach the surface) occurred (Figure 2), mostly along the NERZ, the N120 and the East RZ (Figure 1). Some of them, which we call "intrusions" (e.g., the intrusion that propagated along the NERZ on 17 May 2017), did not lead to an eruption at the surface, but could have had a strong negative effect on the strength of the edifice, via edifice deformation and major stress perturbation, as shown by seismic crises.

2.2. Physical Properties

The distribution of the magnetization and electrical resistivity parameters within the edifice is affected by various factors. Volcanic rocks are generally strongly magnetized, with a predominant thermoremanent component acquired as the rock cools below the Curie temperature. At Piton de la Fournaise, the basaltic lithology is dominated by remanent magnetization (Koenigsberger ratios >1) with a mean value of 10 A m^{-1} inferred from 2D modeling of the Piton de la Fournaise lava flow pile (L.-S. Gailler & Lénat, 2012). In active areas, rock magnetization may be significantly decreased by alteration processes that destroy or transform magnetic minerals into weakly or nonmagnetic minerals, or by increasing the temperature to near or above the Curie temperature, at which point minerals lose their remanent magnetization (e.g., Collinson, 1983). Mechanical heterogeneities, such as inherited fractures that act as pathways for fluids (Bouligand et al., 2020; M. Dumont et al., 2019; L. Gailler & Kauahikaua, 2017), also tend to decrease magnetization. The resistivity of rocks spans several orders of magnitude (J. F. Lénat, 1995) and is determined by their water content, the conductivity and temperature of the fluids, and the presence of hydrated minerals such as clay minerals and zeolites. While massive lava flows are commonly highly resistive, the resistivity is reduced by hydrothermal and magmatic systems, as well as alteration processes (e.g., L. Gailler et al., 2019; Revil et al., 2018, and references therein).

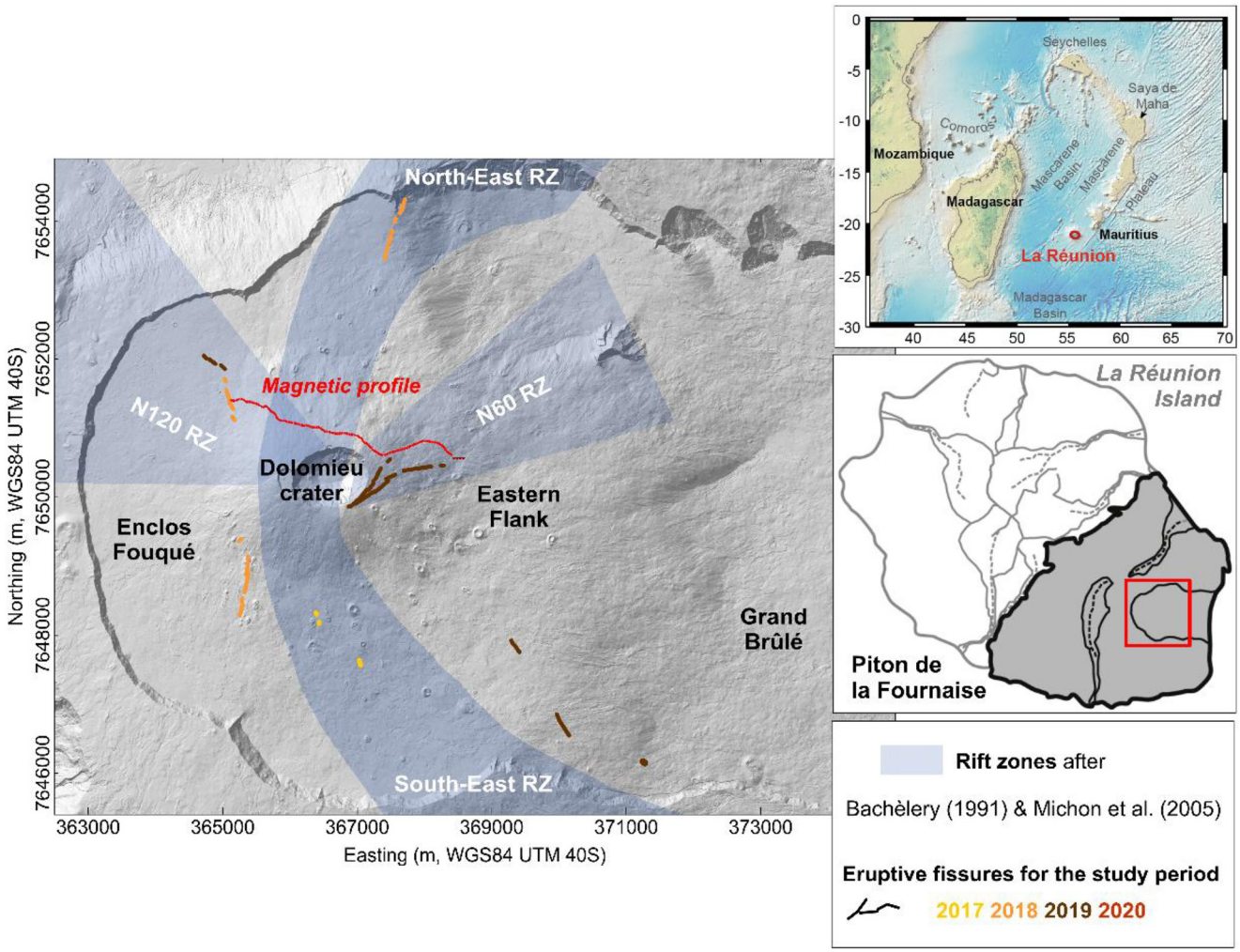

Figure 1. Map of Piton de la Fournaise and its eruptive fissures for the period concerned (from May 2017 to November 2020). Background image: 2010 lidar Digital Elevation Model (DEM).

3. Methodology for Qualitative Analysis of Magnetic Repetitions

3.1. Magnetic Measurements and Data Treatment

Magnetic measurements were acquired during three field surveys in May 2017 (2017a, b, and c), August–September 2019, and November 2020, along a 4-km-long E-W profile (Figures 1 and 3a). The three magnetic surveys were performed using the same portable Overhauser proton-precession magnetometer (GEM GMS19) in walking mode (0.5 s sampling interval), with a sensor mounted on a backpack at a height of about 1.80 m above the ground. The absolute instrumental accuracy was ±0.1 nT. The integrated GPS enables the position to be determined simultaneously while surveying, with a fairly precise (i.e., around 1 m) location of the magnetic measurements even without any postprocessing.

The first survey was performed in May 2017. Measurements were repeated 3 times during this first survey in order to (a) estimate the quality of the measurements and (b) record any variations in the magnetic signal due to magmatic activity at depth. Two reiterations were made before the 17 May 2017 dyke intrusion (2017a and b), and the third one (2017c) just after the intrusion (Figures 2 and 3b). The second survey was carried out in August–September 2019, and the third one in November 2020. The easterly end of the latter profile is not exactly collocated with the previous surveys, because of the presence of lava flows emitted during the 18 February 2019 eruption which were not stable enough to walk on at the time of the survey.

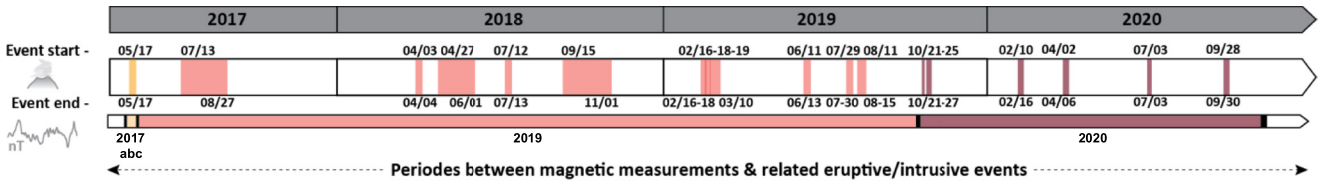

Start		End		*Event*
Day	Time	Day	Time	
05/17/17	16:10	05/17/17	21:00	*Intrusion*
07/13/17	20:50	08/27/17	23:00	*Eruption*
04/03/18	06:40	04/04/18	00:00	*Eruption*
04/27/18	19:50	06/01/18	10:30	*Eruption*
07/12/18	23:30	07/13/18	18:00	*Eruption*
09/15/18	00:25	11/01/18	00:00	*Eruption*
02/16/19	11:21	02/16/19	12:15	*Intrusion*
02/18/19	05:48	02/18/19	18:00	*Eruption*
02/19/19	13:00	03/10/19	02:28	*Eruption*
06/11/19	02:35	06/13/19	08:00	*Eruption*
07/29/19	08:00	07/30/19	00:30	*Eruption*
08/11/19	12:20	08/15/19	00:20	*Eruption*
10/21/19	16:00	10/21/19	16:34	*Intrusion*
10/25/19	10:40	10/27/19	16:30	*Eruption*
02/10/19	06:50	02/16/20	10:12	*Eruption*
04/02/20	08:20	04/06/20	09:30	*Eruption*
07/03/20	03:20	07/03/20	04:00	*Intrusion*
09/28/20	08:04	09/30/20	08:00	*Intrusion*

Figure 2. Chronology of the eruptions and intrusions spanning the May 2017 to November 2020 period. Background colors classify eruptive and intrusive events that occurred between two magnetic measurement reiterations. Color code: yellow, period covered by the 2017a, b, and c surveys; red, period covered by the 2017–2019 surveys; brown, period covered by the 2019–2020 surveys.

Between each series of magnetic surveys, one or more magma injections (certain of which reached the surface) occurred, some of them in the area of the profile, that is, on the N-NE flank of Piton de la Fournaise (Figures 1 and 3). Between the 2017c and 2019 surveys, 12 injections occurred (leading to 10 eruptions and 2 intrusions): 4 are located close to the measurement profile (2 along the N120 RZ, and 2 along the N60 RZ, Figure 1). Between the 2019 and 2020 surveys, six magma injections occurred (three eruptions and three intrusions), with two of them close to the measurement profile on the eastern flank along the N60 RZ (Figure 3a).

Note that short-term variations in magnetic field strength due to various processes in the magnetosphere could not be removed from this study because of the lack of a close-enough magnetic base station. However, although diurnal variations in solar radiation can affect the local magnetic field by approximately 30 nT (e.g., Telford et al., 1990), several studies in similar volcanic contexts have confirmed that daily variations are generally minor (L. Gailler & Kauahikaua, 2017; Zurek & Williams-Jones, 2013) compared to the amplitude of the recorded variations (i.e., more than 1,000 nT). This assumption was confirmed during our surveys, since the difference between the magnetic field values for collocated points in the stable area, during each survey and between them, was less than 50 nT on average. Therefore, no correction was made for the diurnal variation. Magnetic signals are extremely noisy at low elevation above highly active volcanic terrains such as this, with recent lava flows typically exhibiting high-amplitude short-wavelength signals (L. Gailler & Kauahikaua, 2017). This can be explained by their high magnetization, their irregularities at a scale of meters or tens of meters, and the rugged flow surfaces. We also systematically checked on the Intermagnet site to verify that no magnetic storms occurred during the measurement periods. Before each survey, the obvious spikes in the magnetic field data (ranging from about 38,000 to 46,000 nT) were removed manually by a careful visual examination of the overall data sets, on a year by year basis. The high-frequency and short-wavelength signals were then filtered using a spline function, allowing the smoothness and tension to be controlled in the same way for each data set. The best result was obtained with a smoothness and tension of 0.6, similar to a low pass filter at 10–15 m. Any site effect is therefore intrinsically filtered, effectively removing any bias from the distribution and values of the magnetic signal in the profile, and enabling a qualitative analysis to be performed.

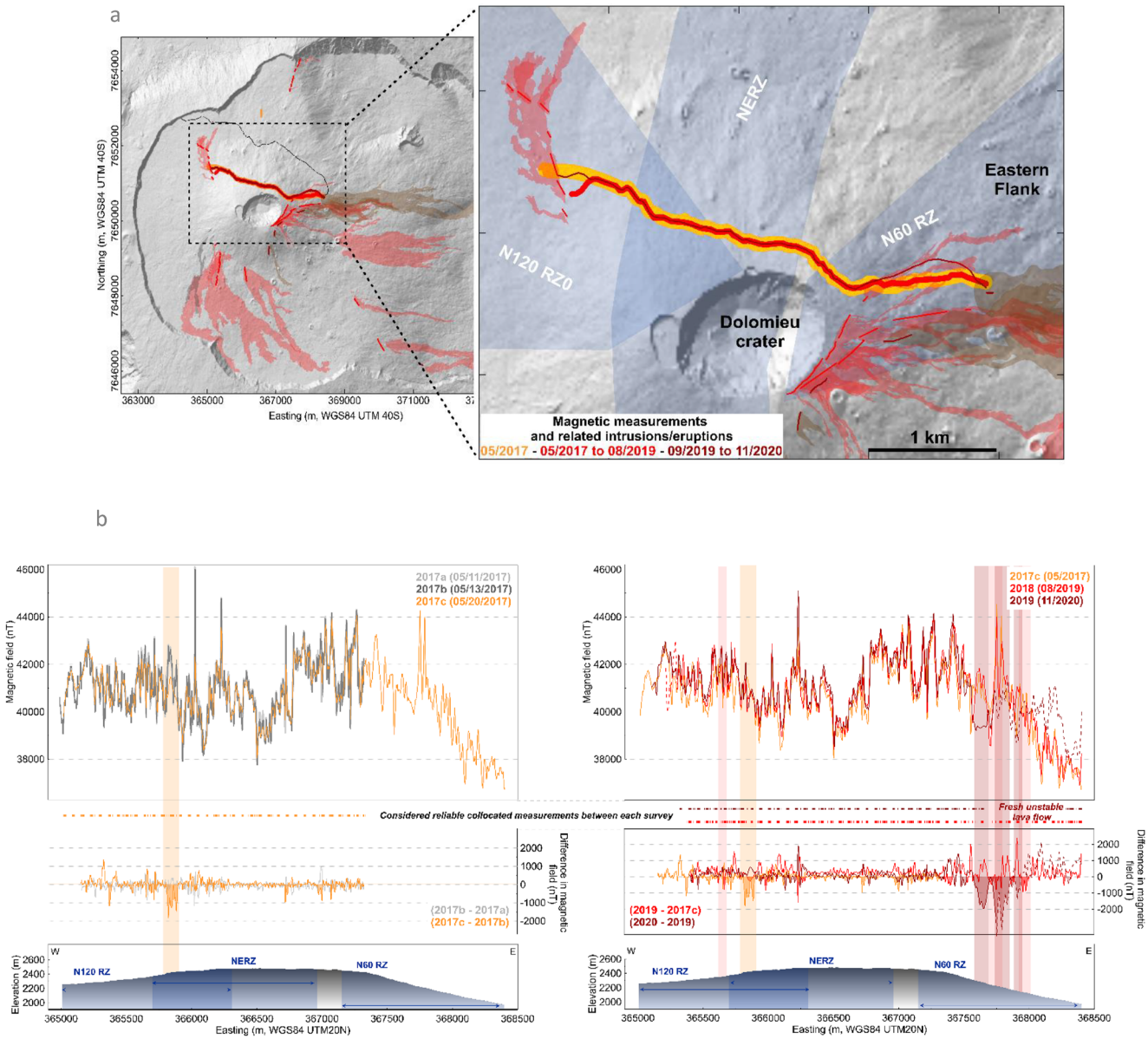

Figure 3. (a) Location of the measurement profile (the eastern part of the 2020 survey is not exactly collocated with the previous ones because the 18 February 2019 eruption area was not stable enough at the time of measurements), lava flows, intrusions axes, and rift zones and (b) associated evolution of the magnetic signal through time. The main decrease in magnetic field is highlighted by shaded areas. Dashed lines show areas where data were not fully collocated along the profile.

The two first sets of the 2017 measurements (2017a and b) were acquired 3 days apart, 3 days before the May 2017 intrusion. They showed a stable magnetic signal, with variations of less than 10 nT on average along the overall profile. On the contrary, a strong decrease of more than 1,000 nT was recorded after the intrusive event (2017c) along the N120 RZ-NERZ area just below the western part of the profile, while the signal remained unchanged especially in the central part of the profile (Figure 3b).

The period between the 2017c and 2019 surveys spanned a larger time than the previous survey period and contained several eruptions and intrusions, of which four eruptions directly affected the area in which the magnetic surveys were carried out on the northern and north-eastern flank of the edifice. In these areas, a decrease in the magnetic signal was observed in 2019 relative to that in 2017c, especially along the N120 RZ, and along the eastern flank in the N60 RZ area, where two magma injections took place in each zone. For the 2020 survey, the eastern end of the profile was not exactly collocated with the previous track, but the decrease recorded in the magnetic signal over this same active area may be significant (Figure 3b). It should be noted

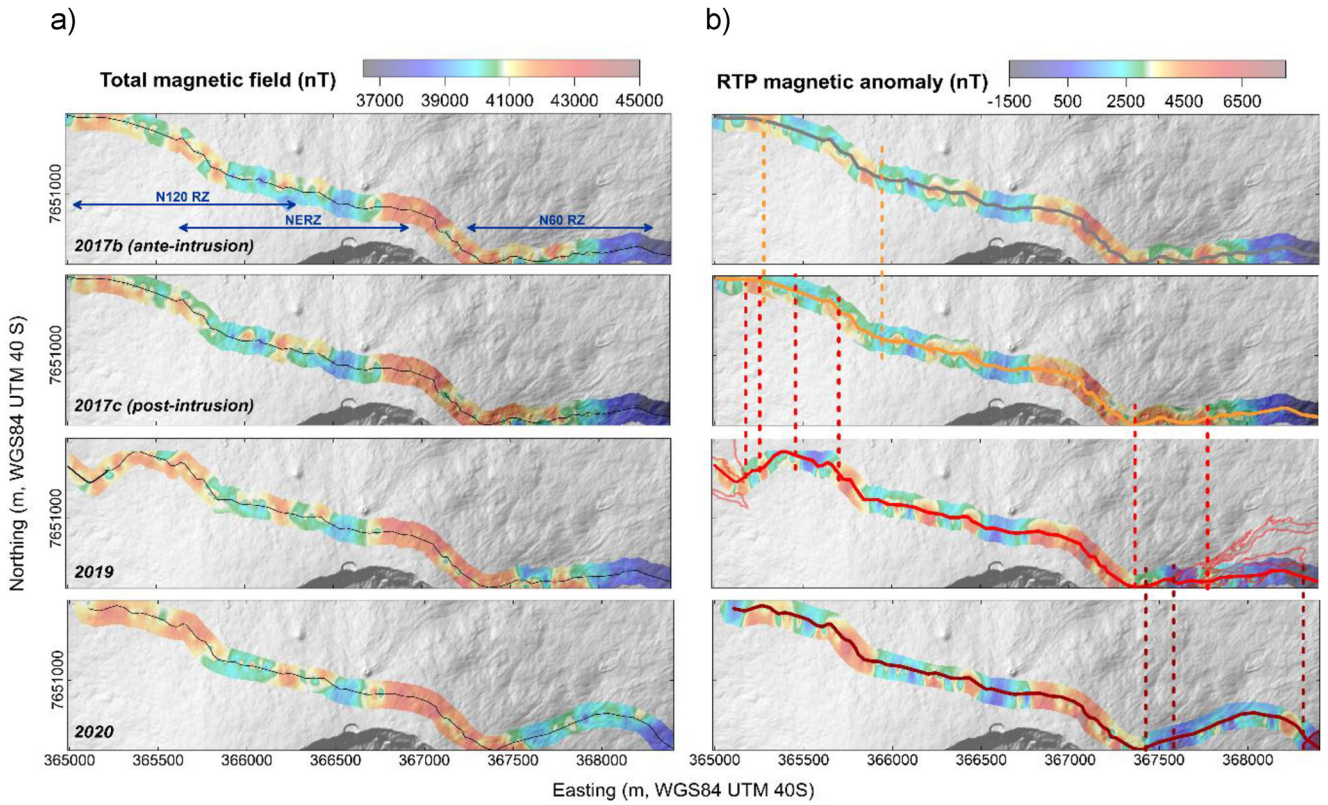

Figure 4. Evolution of the magnetic signal along the reference profile shown as maps: (a) total magnetic field, (b) reduction to the pole (RTP) anomaly, from May 2017 (top) to December 2020 (bottom). The dashed lines in (b) identify the main areas of change in the RTP anomaly from one reiteration to another (see Figure 2 for color code). The data were gridded using the minimum curvature method with a grid spacing of 5 m. Background image: 2010 lidar Digital Elevation Model (DEM).

that the 2019 and 2020 surveys also showed a strong temporal stability in measurements from one data set to another in the central part of the profile. This area was not directly affected by any intrusions or eruptions during the survey period. This observation confirms the high repeatability of the measurements over time and that all significant variations are likely to be related to magmatic processes at depth linked to the eruptive activity.

We then used the variations in the magnetic anomalies to model their spatiotemporal evolution. The magnetic field intensity predicted by the International Geomagnetic Reference Model version 13 (IGRF-13; Alken et al., 2022) was subtracted from the observed values (Figure 4a) to compute the magnetic anomalies. The final postprocessing we applied was a reduction to the pole (RTP; Figure 4b) of the magnetic anomalies in order to reduce the dipolar appearance of the anomalies and shift them to lie above their sources (Baranov, 1957). This transformation requires the directions of the apparent magnetization and the ambient field to be specified (Inclination [I] and Declination [D]). Since we were focusing here on the direct effects of the recent activity at different periods, we used the induced magnetization vector, which is collinear with the ambient field for each period (i.e., the present magnetic field vector in La Réunion: $I = -54.4°$, $D = -19.46°$ in 2017; $I = -54.41°$, $D = -19.38°$ in 2019; $I = -54.28°$, $D = -19.53°$ in 2020). As shown in Figure 4b, it enhanced the decrease in magnetic anomaly (a) between the RZ N120 and the RZ 25–30 after the 2017 intrusion and more locally in 2019 and (b) along the East RZ in 2019 and again in 2020.

3.2. Complementary Methods for Magnetic Modeling and Interpretation

Data sets for two additional methods were used to provide more constraints for our modeling of the magnetic signals and for the discussion: ERT measurements and intrusion geometries derived from inverse modeling of InSAR data.

3.2.1. 2D Electrical Resistivity Tomography

A long ERT profile was acquired simultaneously with the first magnetic data set (Figure 5a). The measurements were performed in May 2017 using an ABEM SAS4000 resistivity meter with 64 electrodes along a 2,520-m-long cable, with the electrodes spaced at 40 m intervals. The total length of the profile was 3,780 m, so the full length was obtained by using one full acquisition (2,520 m long) followed by two roll-alongs each made up of a quarter of the total cable length. The field protocols were the same as those described by Revil et al. (2011). A pole–dipole configuration was used to increase the depth of investigation (Pucci et al., 2016), down to a depth of about 800 m below the surface in its central part. It highlighted the following features: (a) a clear transition from East to West in the summit zone with an increase in resistivity eastward, and (b) a strong influence of the hydrothermal system under the western part of the profile, as also suggested by simultaneous Self-Potential measurements (Barde-Cabusson et al., 2012; M. Dumont et al., 2019).

The complementary nature of magnetic and electrical resistivity methods have been well demonstrated, with, for instance, magnetization being affected by alteration but not by fluid content, and vice versa for electrical resistivity (Bouligand et al., 2016; Brothelande et al., 2016; L. Gailler et al., 2019). Formations with high resistivity will also tend to be highly magnetized in old or unaltered areas. We use this correlation between electrical and magnetization imaging to provide more precise constraints on the geometry of the shallow magnetized layer in our 2D magnetic models.

3.2.2. InSAR Data and 3D Intrusion Imaging

Continuous InSAR monitoring of Piton de la Fournaise has been carried out since 2003 within the framework of the Indian Ocean InSAR Observatory, part of the French National Service ISDeform (INSU/CNRS; Richter & Froger, 2020). Q. Dumont et al. (2022) modeled the displacements caused by the 57 magma injections that occurred between 1998 and 2020 using an approach combining: (a) a 3D Mixed Boundary Element Method (Cayol & Cornet, 1997) that assumes a linearly elastic, homogeneous, and isotropic medium with a realistic topography, and (b) a neighborhood algorithm for exploring the space parameters (Sambridge, 1999). The intrusion geometries were approximated by quadrangular fractures subject to constant overpressure. Here, we use the results of Q. Dumont et al. (2022) to provide additional constraints for our discussion of the observed magnetic changes in terms of volcano-magnetic signals.

3.3. Magnetic Modeling Approach

For each magnetic survey, we calculated 2D direct magnetic models using GMSYS-2D software (© Geosoft) along the profile length. We did this by computing 2D 1/2 models for which the 2D structures were truncated at the same distance in both directions perpendicular to the 2D section. This distance was set to 1 km, which corresponds to the average extent of the main structures observed at the surface along the survey profile. The magnetic model response is based on the method of Talwani and Heirtzler (1964) using the algorithms described in Won and Bevis (1987). Structural units with assigned magnetization values were defined in the direction perpendicular to the profile. Since magnetic models are nonunique, we tested several initial constraints. As mentioned above, the first assumption for our starting model was based on the resistivity distribution derived from the ERT profile (Figure 5a). We considered that the high resistivity layer observed at the surface, interpreted as being massive lava flows, was also highly magnetized. Based on common magnetization values for such basaltic flows, and in agreement with previous models in similar areas, a value of 10 A m^{-1} was used (L.-S. Gailler & Lénat, 2012). This shallow highly resistive and magnetized layer overlies a highly conductive layer that is less magnetized than the surrounding area. Taking into account the effects of the various heterogeneities at this scale (e.g., hydrothermal alteration and faulting) and based on constraints from paleomagnetic studies (Chamalaun, 1968), we used a magnetization value of 2 A m^{-1} for this underlying layer.

4. Results

4.1. Inner Structure Changes Deduced From 2D Modeling of the Volcano-Magnetic Signal

The modeling results are presented in Figure 5. First, note that our initial magnetic model corresponding to the first magnetic survey is in good agreement with the results from the ERT profile for the 2017b data set acquired just before the 17 May 2017 intrusion (Figures 5a and 5b, gray curve). The geometry of the high magnetization

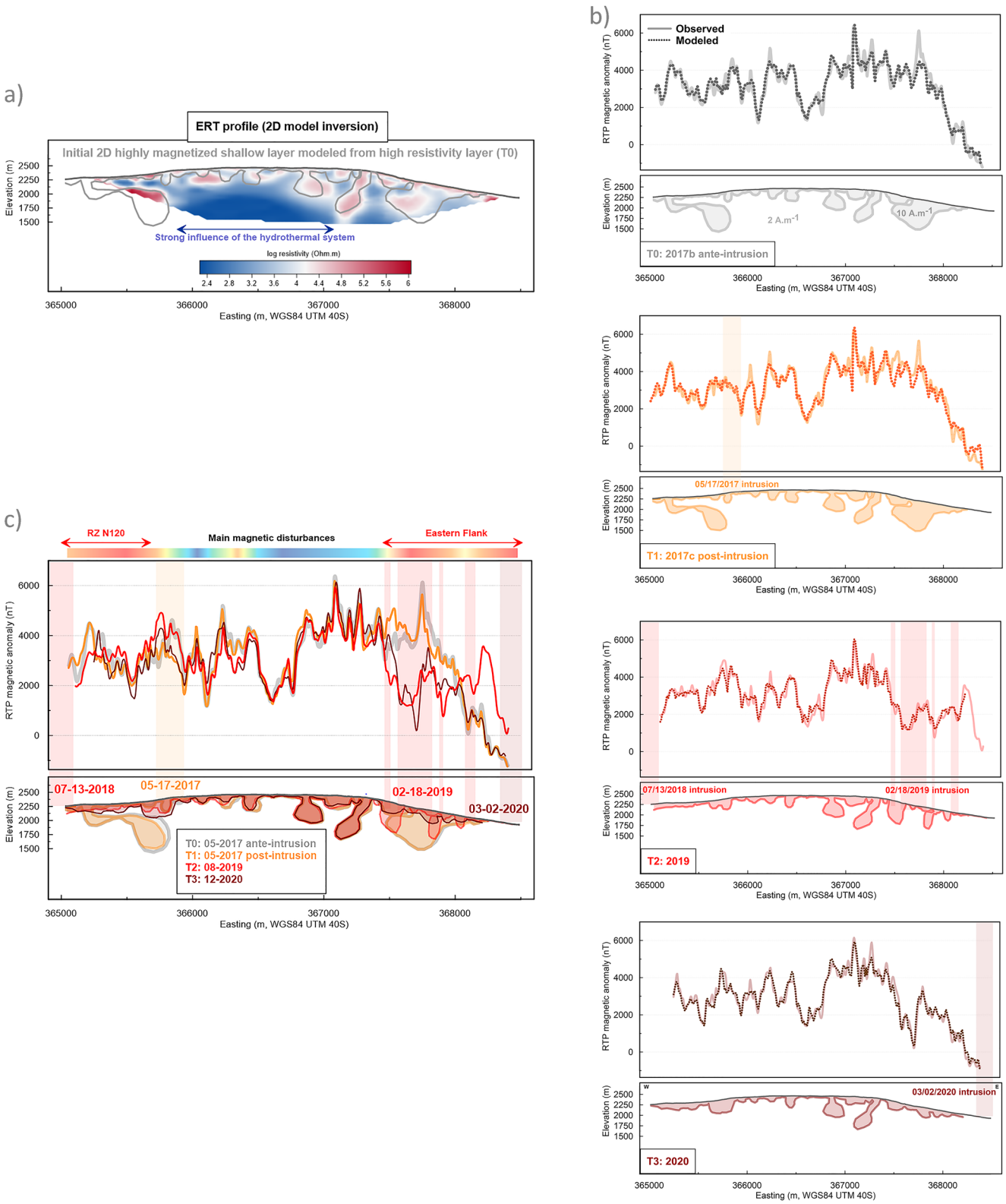

Figure 5. 2D modeling of the evolution of the volcano-magnetic signals from May 2017 to November 2020. (a) 2D model inversion of the SlideVolc electrical resistivity tomography (ERT) profile used as an initial constraint for the geometry of the highly magnetized layer at the surface. (b) 2D magnetic models created using the period of magnetic reiterations. (c) All models superimposed.

and resistivity layer makes it possible to create a good reproduction of most of the anomalies observed at the surface. From this initial model constrained by the electrical resistivity data, we then reconstructed the temporal evolution of the geometry and thickness of the shallow highly magnetized layer for each magnetic survey (i.e., 2017c, 2019, and 2020; Figures 5a and 5b).

It should be stressed that the 17 May 2017 intrusion passed directly beneath the western part of the profile. In this area, the overall extent of the thick magnetized root initially modeled, based on the resistivity tomography (Figure 5a), is slightly reduced (Figures 5b and 5c, orange layer). This demagnetization of the shallow layer is even more striking if we look at the calculated model for the second series of reiterations and its differences to the first model (i.e., comparison between 2017c and 2019 measurements; Figures 5b and 5c, red vs. orange and gray layers). The magnetized root modeled in 2017c (orange layer) at the western side of the profile has completely vanished, with an overall decrease in thickness of the highly magnetized layer (red layer). A similar feature is observed along the eastern flank. The highly magnetized layer (structure B in Figure 5b), modeled as a 500-m-wide root before the 2019 measurements, has become divided into a number of magnetized patches that are less deep. The model for the third survey carried out in 2020 is less clear, but a similar thinning of the magnetized layer is observed below the eastern flank (Figures 5b and 5c, brown layer).

4.2. Comparison With Magma Injections Modeled From InSAR Data

We assume that most of the changes in magnetization between the surveys are related to the magma injected within the edifice during these periods. This assumption can be evaluated by comparing the magnetic signals with the results of InSAR displacements using the model from Q. Dumont et al. (2022) for the intrusions that occurred during each period concerned. This helps evaluate the main spatial variations in magnetic structures and to link them more quantitatively to the volcanic activity (Figure 6).

This observation is most striking for the second survey (Figure 6c). Between the 2017c and 2019 surveys, 12 eruptions/intrusions occurred. Four of the dyke injections modeled from InSAR displacements correlate with changes to the magnetized body (Figure 6c, structure A): the demagnetized area inferred from our 2D models is located along the axis of, or just above, the modeled intrusions at depth. The July 2018 and July 2019 eruptions show shallow dyke/sill rooting at 1,000 m depth and propagation under the NW flank (below the profile) through the previous location of the magnetized root. This clearly suggests the demagnetization effect of these two magma injections on the shallow layer. Similarly, to the east of the Dolomieu crater, the locations of the February and June 2019 magma injections, which trend N60, are clearly consistent with the demagnetized area beneath the eastern flank which separates to either side of the injections. The other magma injections in the 2017–2019 period, as modeled from InSAR displacements, do not seem to have caused significant changes to the magnetized layer, being either too deep or too far from the study area to have had any influence on the magnetic measurements.

Looking at the 2020 measurements (Figure 6d), we observe that two of the four magma injections (October 2019 and September 2020) occurred at great depth (1,000–1,300 m below the surface) and propagated east and south-east, meaning that they had no effect on our profile. However, the February and April 2020 eruptions were fed by injections that emplaced in or near the area imaged by the magnetic profile. In particular, the February 2020 sill, which propagated toward the northeast, is located just below the demagnetized area observed in the eastern part of the profile (structure B), suggesting a possible influence despite its depth. It is also worth noting that, although the dyke models relating to the north-east eruptive fissures of February 2020 and April 2020 have high uncertainties, their possible location intersects the demagnetized zone within a 95% confidence interval, thus possibly explaining it. The thickness of the shallow highly magnetized layer remains unchanged in the absence of any new intrusion.

5. Discussion and Conclusions

Magnetic measurements were carried out over three periods between May 2017 and November 2020 along a reference profile located to the north of the Central Cone at the Piton de la Fournaise. Exactly the same configuration was used for all the surveys (same operator and instrument assembly, sensor at 1.80 m above the ground, sampling frequency at 2 Hz). The data were all reduced using the IGRF, then smoothed and intrinsically filtered from any site effect lower than 10–15 m in order to perform a temporal qualitative analysis. Significant variations (i.e., up to 2,500 nT) were noted in the magnetic signals along the N120 RZ, and even more strikingly along the

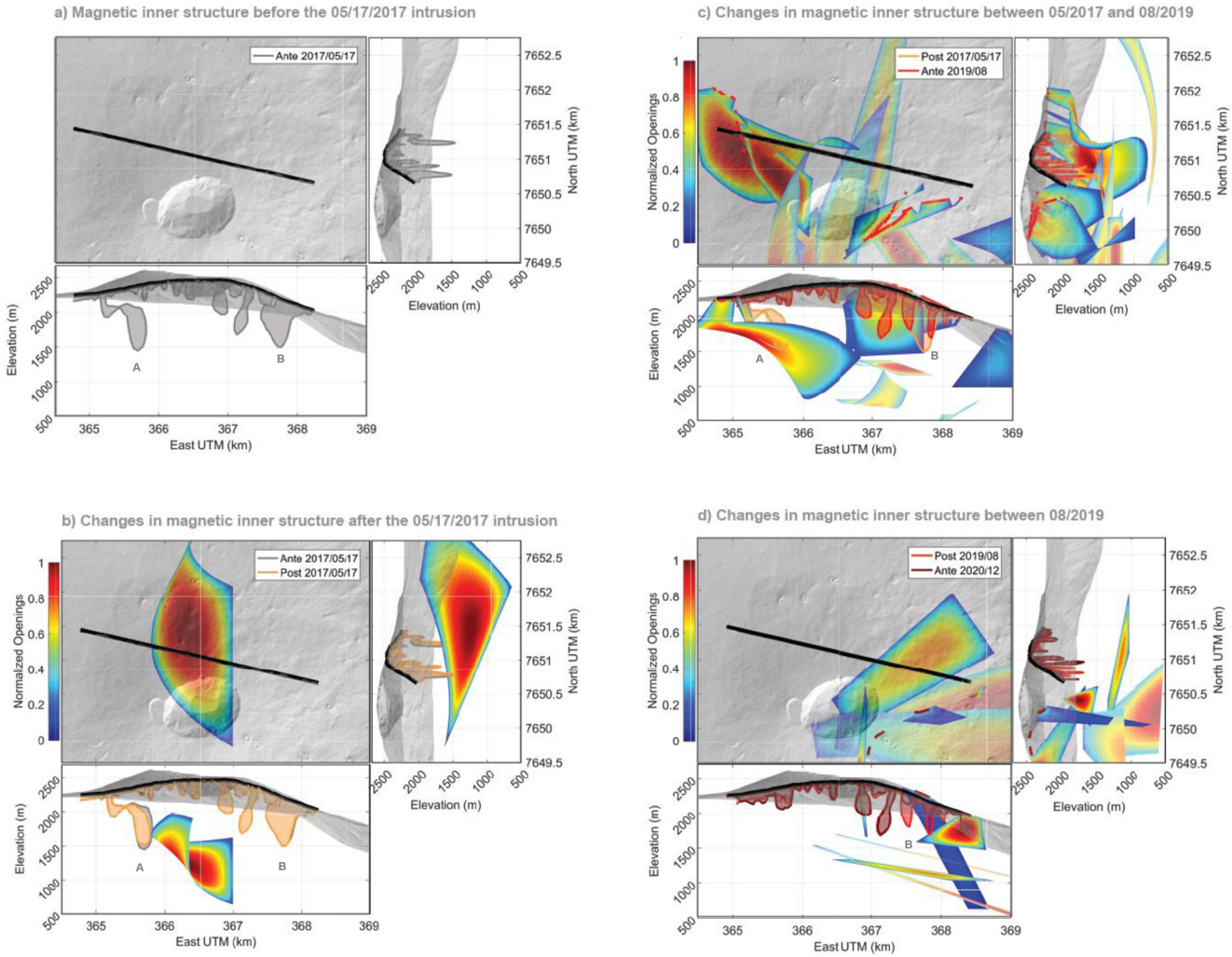

Figure 6. 3D representation of magma transfer derived from Interferometric Synthetic Aperture Radar (InSAR) data inversion versus internal structure changes inferred from magnetic modeling through time for all periods considered (after Q. Dumont et al., 2022): (a) 2017b, (b) 2017c, (c) 2019, and (d) 2020.

eastern flank. We reduced the main negative signals to the pole in order to isolate those demagnetization areas that might be linked to volcano dynamics. The temporal evolution of the magnetic anomalies was then modeled in 2D 1/2 (i.e., considering a symmetrical subsurface structure at right angles to the profile). We assumed a direct correlation between resistivity and magnetization for the initial model, and we focused on demagnetization areas at shallow depth along the main active RZ (N120) and on the eastern flank. In such highly active and complex volcanic contexts, there are numerous phenomena that could generate such magnetization and magnetic field variations, all of which can occur simultaneously:

1. *Thermomagnetic effects*: magma intrusions are associated with high thermal conditions, and the temperature often exceeds the Curie temperature (i.e., 580°C), thus resulting in thermal demagnetization.
2. *Piezomagnetic effects*: thermal variations are commonly associated with stress variations (piezomagnetism) caused by the injection of new material into the edifice.
   In our study, much of the magnetized rock at shallow depth exhibits a change in magnetic properties in areas where InSAR models indicate that dykes are present. This suggests that at least part of the observed volcano-magnetic variation may be due to thermal demagnetization of the rocks caused by a combination of thermomagnetism and piezomagnetic effects.
3. *Electrokinetic variations*: the heat and gases associated with magma injection alter the circulation of fluids (e.g., J.-F. Lénat, Bachèlery, & Peltier, 2012), generating electrokinetic variations that could also affect the magnetization of the overall system.

Numerous electrical and magnetic signals attributed to electrokinetic effects have been already documented for Piton de la Fournaise (see Adler et al., 1999, and references therein), associated with fluid circulation (e.g., Fitterman, 1979; Mizutani et al., 1976; Zlotnicki & Le Mouél, 1990). Generalized electrokinetic perturbation of the whole system, geometrically through fracturing, and chemically by volcanic fluids, is thought to have occurred along the N120 RZ and the eastern flank. Other inherited fractures can also provide preferential paths for hydrothermal and magma circulation, leading to disruption of the signals.

These results opened up a new approach in the study of spatiotemporal changes in magmatic and mechanical variations, and hydrothermal alteration processes within volcano edifices. To improve our understanding of the spatiotemporal change rate of the magnetization parameters, we recently coupled these ground measurements with high-resolution Unmanned Aerial Vehicle magnetic surveys (L. Gailler, Labazuy, Régis, et al., 2022). This is the first time that this method has been used in this location, and it represents a considerable advance, making the spatiotemporal monitoring more efficient at different scales (homogeneous cover, exact and precise reiterations, rapid and safe sampling in otherwise inaccessible areas). The additional information from this near-real time analysis of the magnetic signal will allow for rapid identification of the dynamics of the magnetic phenomena and better quantification of the demagnetization rate and its origin due to volcanic activity.

To conclude, this study confirms that the detection of magnetization (and electrical resistivity) anomalies and the quantification of their spatiotemporal evolution (i.e., in 4D) are powerful tools in imaging volcano systems at various temporal and spatial scales. An interesting future development would be to use direct modeling to simulate the changes in magnetic signals from dyke models derived from InSAR, and then to perform joint magnetic/deformation inversions in order to better constrain the geometry of dyke/sill injections.

Appendix A

The SlideVolc ERT Team: Nicolas Cluzel, Eric Delcher, Jean-Michel Dulong, Giulia Del Manzo, Florian Durand, Brice Foucart, Alicia Gonzales, Jonas Greve, Elsa Gonano, Bastien Joly, Rachel Gusset, Mazhar Meralli Ballou, Laurent Perrier, Brice Robert, Robert Scholz, and Fanny Soler.

Data Availability Statement

The data presented in this study can be found online: https://doi.org/10.5281/zenodo.6938137 (L. Gailler, Labazuy, Dumont, et al., 2022). InSAR data were acquired within the framework of the Indian Ocean InSAR Observatory (OI2/OPGC/SNOV/INSU), where the interferograms used in this study are available on the CASOAR link (https://wwwobs.univ-bpclermont.fr/casoar). Licensed commercial software has been used for geophysical data modeling and visualization: © Res2DInv (Aarhus Geosoftware), © Oasis Montaj (Geosoft), and © Golden Surfer. InSAR data inversions were performed on the supercomputer facilities of the Mésocentre Clermont-Auvergne.

Acknowledgments
The ERT survey and the first magnetic measurements were funded by The French National Agency for Research (ANR contract 16-CE04-0004-01 SlideVOLC). The follow-up magnetic reiteration surveys and the presented study were funded by the Centre National d'Études Spatiales (CNES), by the Laboratory of Excellence ClerVolc and the ANR Scan4Volc. We are grateful to the staff of the Observatoire Volcanologique du Piton de la Fournaise from Institut de Physique du Globe de Paris (OVPF-IPGP) and Raphaël Antoine (Cerema) for their support throughout the field work and for fruitful discussions. We also warmly acknowledge the Parc National de la Réunion and InAirTech. The editors, Douglas Schmitt and Agnes Kontny, and the two reviewers, Bill Moris and an anonymous one, are acknowledged for their constructive comments and annotations that improved the quality of the manuscript. This is Laboratory of Excellence ClerVolc contribution number 555.

References

Adler, P. M., Le Mouel, J. L., & Zlotnicki, J. (1999). Electrokinetic and magnetic fields generated by flow through a fractured zone: A sensitivity study for La Fournaise volcano. *Geophysical Research Letters*, *26*(6), 795–798. https://doi.org/10.1029/1999GL900095

Alken, P., Thébault, E., Beggan, C. D., & Nosé, M. (2022). Special issue "International Geomagnetic Reference Field: The thirteenth generation". *Earth, Planets and Space*, *74*(1), 11–14. https://doi.org/10.1186/s40623-021-01569-z

Bachèlery, P. (1981). *Le Piton de la Fournaise (île de la Réunion). Etude Volcanologique, Structurale et Pétrologique*. Université de Clermont-Ferrand.

Baranov, W. (1957). A new method for interpretation of aeromagnetic maps: Pseudo-gravimetric anomalies. *Geophysics*, *22*(2), 359–383. https://doi.org/10.1190/1.1438369

Barde-Cabusson, S., Finizola, A., Peltier, A., Chaput, M., Taquet, N., Dumont, S., et al. (2012). Structural control of collapse events inferred by self-potential mapping on the Piton de la Fournaise volcano (La Réunion Island). *Journal of Volcanology and Geothermal Research*, *209–210*, 9–18. https://doi.org/10.1016/j.jvolgeores.2011.09.014

Bonali, F. L., Corazzato, C., & Tibaldi, A. (2011). Identifying rift zones on volcanoes: An example from La Réunion Island, Indian Ocean. *Bulletin of Volcanology*, *73*(3), 347–366. https://doi.org/10.1007/s00445-010-0416-1

Bouligand, C., Coutant, O., & Glen, J. M. G. (2016). Sub-surface structure of La Soufrière of Guadeloupe lava dome deduced from a ground-based magnetic survey. *Journal of Volcanology and Geothermal Research*, *321*, 171–181. https://doi.org/10.1016/j.jvolgeores.2016.04.037

Bouligand, C., Hurwitz, S., Vandemeulebrouck, J., Byrdina, S., Kass, M. A., & Lewicki, J. L. (2019). Heat and mass transport in a vapor-dominated hydrothermal area in Yellowstone National Park, USA: Inferences from magnetic, electrical, electromagnetic, subsurface temperature, and diffuse CO_2 flux measurements. *Journal of Geophysical Research: Solid Earth*, *124*, 291–309. https://doi.org/10.1029/2018JB016202

Bouligand, C., Tivey, M. A., Finn, C. A., Iii, W. C. P. S., & Sohn, R. A. (2020). Geological and thermal control of the hydrothermal system in northern Yellowstone lake: Inferences from high-resolution magnetic surveys. *Journal of Geophysical Research: Solid Earth*, *125*, e2020JB019743. https://doi.org/10.1029/2020JB019743

Brothelande, E., Lénat, J.-F., Chaput, M., Gailler, L., Finizola, A., Dumont, S., et al. (2016). Structure and evolution of an active resurgent dome evidenced by geophysical investigations: The Yenkahe dome-Yasur volcano system (Siwi caldera, Vanuatu). *Journal of Volcanology and Geothermal Research*, *322*, 241–262. https://doi.org/10.1016/j.jvolgeores.2015.08.021

Cayol, V., & Cornet, F. H. (1997). 3D mixed boundary elements for elastostatic deformation field analysis. *International Journal of Rock Mechanics and Mining Science & Geomechanics Abstracts*, *34*(2), 275–287. https://doi.org/10.1016/S0148-9062(96)00035-6

Chamalaun, F. H. (1968). Paleomagnetism of Réunion island and its bearing on secular variation. *Journal of Geophysical Research*, *73*(14), 4647–4659. https://doi.org/10.1029/JB073i014p04647

Chaput, M., Finizola, A., Peltier, A., Villeneuve, N., Crovisier, M., & Barde-Cabusson, S. (2019). Where does a volcano break? Using self-potential reiteration to forecast the precise location of major destructive events on active volcanoes: The case study of the Piton de la Fournaise 2007 caldera collapse. *Volcanica*, *2*, 151–159. https://doi.org/10.30909/vol.02.02.151159

Chevrel, M. O., Favalli, M., Villeneuve, N., Harris, A. J. L., Fornaciai, A., Richter, N., et al. (2021). Lava flow hazard map of Piton de la Fournaise volcano. *Natural Hazards and Earth System Sciences*, *21*(8), 2355–2377. https://doi.org/10.5194/nhess-21-2355-2021

Collinson, D. W. (1983). Methods in rock magnetism and palaeomagnetism. https://doi.org/10.1007/978-94-015-3979-1

Dumont, Q., Cayol, V., Froger, J., & Peltier, A. (2022). Major destabilization structure revealed by 22 years of satellite imagery at Piton de la Fournaise. *Nature Communications*, *13*, 1–11. https://doi.org/10.1038/s41467-022-30109-w

Dumont, M., Peltier, A., Roblin, E., Reninger, P. A., Barde-Cabusson, S., Finizola, A., & Ferrazzini, V. (2019). Imagery of internal structure and destabilization features of active volcano by 3D high resolution airborne electromagnetism. *Scientific Reports*, *9*, 1–11. https://doi.org/10.1038/s41598-019-54415-4

Finizola, A., Aubert, M., Revil, A., Schütze, C., & Sortino, F. (2009). Importance of structural history in the summit area of Stromboli during the 2002–2003 eruptive crisis inferred from temperature, soil CO_2, self-potential, and electrical resistivity tomography. *Journal of Volcanology and Geothermal Research*, *183*(3–4), 213–227. https://doi.org/10.1016/j.jvolgeores.2009.04.002

Fitterman, D. V. (1979). Theory of electrokinetic-magnetic anomalies in a faulted half-space. *Journal of Geophysical Research*, *84*(B11), 6031–6040. https://doi.org/10.1029/JB084iB11p06031

Froger, J.-L., Famin, V., Cayol, V., Augier, A., Michon, L., & Lénat, J.-F. (2015). Time-dependent displacements during and after the April 2007 eruption of Piton de la Fournaise, revealed by interferometric data. *Journal of Volcanology and Geothermal Research*, *296*, 55–68. 10.1016/j.jvolgeores.2015.02.014

Fukushima, Y., Cayol, V., Durand, P., & Massonnet, D. (2010). Evolution of magma conduits during the 1998–2000 eruptions of Piton de la Fournaise volcano, Réunion Island. *Journal of Geophysical Research*, *115*, B10204. https://doi.org/10.1029/2009JB007023

Gailler, L., & Kauahikaua, J. (2017). Monitoring the cooling of the 1959 Kīlauea Iki lava lake using surface magnetic measurements. *Bulletin of Volcanology*, *79*(6), 40. https://doi.org/10.1007/s00445-017-1119-7

Gailler, L., & Kauahikaua, J. (2018). The gravity signature of basaltic fill in Kīlauea caldera, Island of Hawai'i. In *GSA books* (Vol. 538, pp. 297–306). https://doi.org/10.1130/2018.2538(13)

Gailler, L., Kauahikaua, J., Lénat, J.-F., Revil, A., Gresse, M., Ahmed, A. S., et al. (2019). 3D electrical conductivity imaging of Halema'uma'u lava lake (Kīlauea volcano). *Journal of Volcanology and Geothermal Research*, *381*, 185–192. https://doi.org/10.1016/j.jvolgeores.2019.06.001

Gailler, L., Labazuy, P., Dumont, Q., Froger, J.-L., Peltier, A., Finizola, A., et al. (2022). Total magnetic field measurements Piton de la Fournaise 2017–2019–2020 (version 1) [Dataset]. Zenodo. https://doi.org/10.5281/zenodo.6938137

Gailler, L., Labazuy, P., Régis, E., Peltier, A., & Ferrazzini, V. (2022). Active structures and thermal state of the Piton de la Fournaise summit area revealed by combined UAV magnetic and IR measurements. *Volcanica*, *5*(1), 61–74. https://doi.org/10.30909/vol.05.01.6174

Gailler, L., Lénat, J. F., Lambert, M., Levieux, G., Villeneuve, N., & Froger, J. L. (2009). Gravity structure of Piton de la Fournaise volcano and inferred mass transfer during the 2007 crisis. *Journal of Volcanology and Geothermal Research*, *184*(1–2), 31–48. https://doi.org/10.1016/j.jvolgeores.2009.01.024

Gailler, L.-S., & Lénat, J.-F. (2012). Internal architecture of La Réunion (Indian Ocean) inferred from geophysical data. *Journal of Volcanology and Geothermal Research*, *221–222*, 221–222. https://doi.org/10.1016/j.jvolgeores.2012.01.015

Gailler, L.-S., Martí, A., & Lénat, J.-F. (2018). Complex structure of Piton de la Fournaise and its underlying lithosphere revealed by magnetotelluric 3D inversion. *Journal of Volcanology and Geothermal Research*, *356*, 200–210. https://doi.org/10.1016/j.jvolgeores.2018.03.006

Galdéano, A., Lénat, J.-F., & Lalanne, F.-X. (1988). Carte magnétique de l'île de la Réunion.

Labazuy, P. (1996). Recurrent landslides events on the submarine flank of Piton de la Fournaise volcano (Réunion Island). In W. McGuire, A. P. Jones, & J. Neuberg (Eds.), *Volcano instability on the Earth and other planets*. (pp. 293–305). Geological Society Special Publication.

Labazuy, P., Gouhier, M., Harris, A., Guéhenneux, Y., Hervo, M., Bergès, J. C., et al. (2012). Near real-time monitoring of the April–May 2010 Eyjafjallajökull ash cloud: An example of a web-based, satellite data-driven, reporting system. *International Journal of Environment and Pollution*, *48*, 262–272. https://doi.org/10.1504/IJEP.2012.049673

Lénat, J. F. (1995). Geoelectrical methods in volcano monitoring. In W. McGuire, C. R. J. Kilburn, & J. B. Murray (Eds.), *Monitoring active volcanoes: Strategies, procedures and techniques* (pp. 248–274). UCL Press.

Lénat, J. F., & Bachèlery, P. (1988). Dynamics of magma transfers at Piton de la Fournaise volcano (Réunion Island, Indian Ocean). In Chi-Yu & R. Scarpa (Eds.), *Earth Evolution Sciences. Special Issue "Modeling of Volcanic Processes"* (pp. 57–72). Friedrich Vieweg & Sohn.

Lénat, J.-F., & Bachèlery, P. (1990). Structure et fonctionnement de la zone centrale du Piton de la Fournaise. In J.-F. Lénat (Ed.), *Le Volcanisme de La Réunion Monographie* (pp. 257–296). Centre de RecherchesVolcanologiques.

Lénat, J.-F., Bachèlery, P., & Merle, O. (2012). Anatomy of Piton de la Fournaise volcano (La Réunion, Indian Ocean). *Bulletin of Volcanology*, *74*(9), 1945–1961. https://doi.org/10.1007/s00445-012-0640-y

Lénat, J.-F., Bachèlery, P., & Peltier, A. (2012). The interplay between collapse structures, hydrothermal systems and magma intrusions: The case of the central area of Piton de la Fournaise volcano. *Bulletin of Volcanology*, *74*(2), 407–421. https://doi.org/10.1007/s00445-011-0535-3

Lipman, P., Normark, W., Moore, J., Wilson, J., & Gutmacher, C. (1988). The giant submarine Alika debris slide, Mauna Loa, Hawaii. *Journal of Geophysical Research*, *93*(B5), 4279–4299. https://doi.org/10.1029/JB093iB05p04279

MacDonald, G. A. (1972). *Volcanoe*s (510 pp.). Prentice-Hall.

Malengreau, B., Lénat, J. F., & Froger, J. L. (1999). Structure of Reunion Island (Indian Ocean) inferred from the interpretation of gravity anomalies. *Journal of Volcanology and Geothermal Research*, *88*(3), 131–146. https://doi.org/10.1016/s0377-0273(98)00114-0

Michon, L., Ferrazzini, V., & Di Muro, A. (2016). Magma paths at Piton de la Fournaise volcano. In B. Patrick, L. Jean-François, D. M. Andrea, & M. Laurent (Eds.), *Active volcanoes of the Southwest Indian Ocean: Piton de la Fournaise and Karthala, active volcanoes of the world* (pp. 91–106). Springer. https://doi.org/10.1007/978-3-642-31395-0_7

Michon, L., Ferrazzini, V., Di Muro, A., Villeneuve, N., & Famin, V. (2015). Rift zones and magma plumbing system of Piton de la Fournaise volcano: How do they differ from Hawaii and Etna? *Journal of Volcanology and Geothermal Research*, *303*, 112–129. https://doi.org/10.1016/j.jvolgeores.2015.07.031

Millington, S. C., Saunders, R. W., Francis, P. N., & Webster, H. N. (2012). Simulated volcanic ash imagery: A method to compare NAME ash concentration forecasts with SEVIRI imagery for the Eyjafjallajökull eruption in 2010. *Journal of Geophysical Research*, *117*, D00U17. https://doi.org/10.1029/2011JD016770

Mizutani, H., Ishido, T., Yokokura, T., & Ohnishi, S. (1976). Electrokinetic phenomena associated with earthquakes. *Geophysical Research Letters*, *3*(7), 365–368. https://doi.org/10.1029/GL003i007p00365

Moore, J. G., Normark, W. R., & Holcomb, R. T. (1994). Giant Hawaiian landslides. *Annual Review of Earth and Planetary Sciences*, *22*(1), 119–144. https://doi.org/10.1146/annurev.ea.22.050194.001003

Nicolosi, I., Caracciolo, F. D., Branca, S., Ventura, G., & Chiappini, M. (2014). Volcanic conduit migration over a basement landslide at Mount Etna (Italy). *Scientific Reports*, *4*(1), 5293. https://doi.org/10.1038/srep05293

Oehler, J.-F., Labazuy, P., & Lénat, J.-F. (2004). Recurrence of major flank landslides during the last 2-Ma-history of Reunion Island. *Bulletin of Volcanology*, *66*(7), 585–598. https://doi.org/10.1007/s00445-004-0341-2

Peltier, A., Bachèlery, P., & Staudacher, T. (2009). Magma transport and storage at Piton de la Fournaise (La Réunion) between 1972 and 2007: A review of geophysical and geochemical data. *Journal of Volcanology and Geothermal Research*, *184*(1–2), 93–108. https://doi.org/10.1016/j.jvolgeores.2008.12.008

Peltier, A., Ferrazzini, V., Staudacher, T., & Bachèlery, P. (2005). Imaging the dynamics of dyke propagation prior to the 2000–2003 flank eruptions at Piton de la Fournaise, Reunion Island. *Geophysical Research Letters*, *32*, L22302. https://doi.org/10.1029/2005GL023720

Pucci, S., Civico, R., Villani, F., Ricci, T., Delcher, E., Finizola, A., et al. (2016). Deep electrical resistivity tomography along the tectonically active Middle Aterno Valley (2009 L'Aquila earthquake area, central Italy). *Geophysical Journal International*, *207*(2), 967–982. https://doi.org/10.1093/gji/ggw308

Revil, A., Finizola, A., Ricci, T., Delcher, E., Peltier, A., Barde-Cabusson, S., et al. (2011). Hydrogeology of Stromboli volcano, Aeolian Islands (Italy) from the interpretation of resistivity tomograms, self-potential, soil temperature and soil CO_2 concentration measurements. *Geophysical Journal International*, *186*(3), 1078–1094. https://doi.org/10.1111/j.1365-246X.2011.05112.x

Revil, A., Ghorbani, A., Gailler, L. S., Gresse, M., Cluzel, N., Panwar, N., & Sharma, R. (2018). Electrical conductivity and induced polarization investigations at Kilauea volcano, Hawai'i. *Journal of Volcanology and Geothermal Research*, *368*, 31–50. https://doi.org/10.1016/j.jvolgeores.2018.10.014

Richter, N., & Froger, J. L. (2020). The role of Interferometric Synthetic Aperture Radar in detecting, mapping, monitoring, and modelling the volcanic activity of Piton de la Fournaise, La Reunion: A review. *Remote Sensing*, *12*(6), 1019. https://doi.org/10.3390/rs12061019

Sambridge, M. (1999). Geophysical inversion with a neighbourhood algorithm—I. Searching a parameter space. *Geophysical Journal International*, *138*(2), 479–494. https://doi.org/10.1046/j.1365-246X.1999.00876.x

Smittarello, D., Cayol, V., Pinel, V., Peltier, A., Froger, J. L., & Ferrazzini, V. (2019). Magma propagation at Piton de la Fournaise from joint inversion of InSAR and GNSS. *Journal of Geophysical Research: Solid Earth*, *124*, 1361–1387. https://doi.org/10.1029/2018JB016856

Swanson, D. A., Rose, T. R., Fiske, R. S., & McGeehin, J. P. (2012). Keanakāko'i Tephra produced by 300 years of explosive eruptions following collapse of Kīlauea Caldera in about 1500 CE. *Journal of Volcanology and Geothermal Research*, *215–216*, 8–25. https://doi.org/10.1016/j.jvolgeores.2011.11.009

Talwani, M., & Heirtzler, J. R. (1964). Computation of magnetic anomalies caused by two-dimensional bodies of arbitrary shape. In G. A. Parks (Ed.), *Computers in the mineral industries, Part 1: Stanford University Publications, Geological Sciences* (pp. 464–480).

Telford, W. M., Geldart, L. P., & Sheriff, L. E. (1990). Chapter 2: Gravity methods. Chapter 3: Magnetic methods. In *Applied geophysics* (2nd ed., pp. 6–61, 62–135). Cambridge University Press.

Villeneuve, N., & Bachèlery, P. (2006). Review of volcanic eruption typology at the Piton de la Fournaise, processes and hazards. *Cybergeo: European Journal of Geography*. https://doi.org/10.4000/cybergeo.2536

Won, I. J., & Bevis, M. (1987). Computing the gravitational and magnetic anomalies due to a polygon: Algorithms and Fortran subroutines. *Geophysics*, *52*(2), 232–238. https://doi.org/10.1190/1.1442298

Zlotnicki, J., Delmond, J. C., Pambrun, C., & Delorme, H. (1993). Magnetic variations on Piton de la Fournaise volcano. Volcanomagnetic signals associated with the November 6 and 30, 1987, eruptions 56.

Zlotnicki, J., & Le Mouel, J. L. (1988). Volcanomagnetic effects observed on Piton de la Fournaise volcano (Reunion Island): 1985–1987. *Journal of Geophysical Research*, *93*(B8), 9157–9171. https://doi.org/10.1029/JB093iB08p09157

Zlotnicki, J., & Le Mouél, J. L. (1990). Possible electrokinetic origin of large magnetic variations at La Fournaise volcano. *Nature*, *343*(6259), 633–636. https://doi.org/10.1038/343633a0

Zurek, J., & Williams-Jones, G. (2013). The shallow structure of Kīlauea caldera from high-resolution Bouguer gravity and total magnetic anomaly mapping: Insights into progressive magma reservoir growth. *Journal of Geophysical Research: Solid Earth*, *118*, 3742–3752. https://doi.org/10.1002/jgrb.50243